Powder Technology 208 (2011) 279–288

Contents lists available at ScienceDirect

Powder Technology

journal homepage: www.elsevier.com/locate/powtec

Polygons vs. clumps of discs: A numerical study of the influence of grain shape on the mechanical behaviour of granular materials ☆

K. Szarf, G. Combe *, P. Villard

Université de Grenoble, Laboratoire Sols, Solides, Structures, Risques (3SR) UJF, G-INP, CNRS UMR 5521, Domaine Universitaire BP53 38041 Grenoble Cedex 9, France

ARTICLE INFO

Keywords:
Granular materials
DEM
Grain shape
Clumps of discs
Polygons
Shear localisation

ABSTRACT

We performed a series of numerical vertical compression tests on assemblies of 2D granular material using a Discrete Element code and studied the results with regard to the grain shape. The samples consist of 5000 grains made from either 3 overlapping discs (clumps — grains with concavities) or six-edged polygons (convex grains). These two grain type have similar external envelope, which is a function of a geometrical parameter α.
In this paper, the numerical procedure applied is briefly presented followed by the description of the granular model used. Observations and mechanical analysis of dense and loose granular assemblies under isotropic loading are made. The mechanical response of our numerical granular samples is studied in the framework of the classical vertical compression test with constant lateral stress (biaxial test). The comparison of macroscopic responses of dense and loose samples with various grain shapes shows that when α is considered a concavity parameter, it is therefore a relevant variable for increasing mechanical performances of dense samples. When α is considered an envelope deviation from perfect sphericity, it can control mechanical performances for large strains. Finally, we present some remarks concerning the kinematics of the deformed samples: while some polygon samples subjected to a vertical compression present large damage zones (any polygon shape), dense samples made of clumps always exhibit thin reflecting shear bands.

1. Introduction

A typical numerical approach to discrete element modeling of granular materials is to use simple shapes of particles (discs in 2D [1] or spheres in 3D [2]). Although the computation time is short using this method, these models cannot reflect some of the more complex aspects of real granular media behaviour, such as high shear resistance or high volumetric changes [3]. In order to model these mechanisms properly, physical phenomena (resistance to inter-granular rolling [4–6]) or other grain shapes (sphere aggregates [7] or polyhedral grains [8]) must be used. The influence of grain shape is not yet fully understood. In this article, we will present our findings concerning the influence of grain shape (grain concavity in particular) on the mechanical behaviour of granular assemblies. We compared two groups of grains — convex irregular polygons and non-convex aggregates of three overlapping discs.

2. Granular model

The granular model used consists of 5000 polydisperse 2D frictional particles. Two kinds of grain shape are used: convex irregular polygons with six edges and non-convex particles made of aggregates of three overlapping discs called *clumps*. These two shapes were chosen because of the similarity of their global contour (polygonal grains can be seen as a polygonal envelope of clumps made of three discs). As shown in Fig. 1, particle shape is defined by a parameter $\alpha = \frac{\Delta R}{R_1}$, where R_1 denotes the ex-circle radius of the particle and ΔR is the difference between the ex-circle and the in-circle radii, [9,10]. The in-circle must be fully contained in the particle. For non-convex clumps, α ranges from 0 (circle) to 0.5. For convex polygonal grains, α ranges from $1-\frac{\sqrt{3}}{2} \simeq 0.13$ (regular hexagons) to 0.5 (equilateral triangles). Some of the shapes used are presented at the bottom of Fig. 1. For each chosen α, granular samples are made of polydisperse particles: the polydispersity of grains is determined by the radii of the grain ex-circle. In each sample, the chosen radii R_1 are such that the areas of the ex-circles are equally distributed between $S_m = \pi(R_m)^2$ and $S_M = \pi(R_M)^2 = \pi(3R_m)^2$.

3. Discrete Element Method

Two-dimensional numerical simulations were carried out using the Discrete Element Method according to the principles of *Molecular Dynamics* (MD) [11]. Two codes were used: PFC^{2D} by ITASCA [12] for clump simulation and a code capable of dealing with polygonal particles that was developed at the laboratory. Both codes use the same contact laws for contact forces computations [13]: grains interact in their contact points with a linear elastic law and Coulomb friction. The normal

☆ This paper was written as part of a CEGEO research project (http://www.granuloscience.com/CEGEO/).
* Corresponding author.
E-mail address: gael.combe@ujf-grenoble.fr (G. Combe).

0032-5910/$ – see front matter © 2010 Elsevier B.V. All rights reserved.
doi:10.1016/j.powtec.2010.08.017

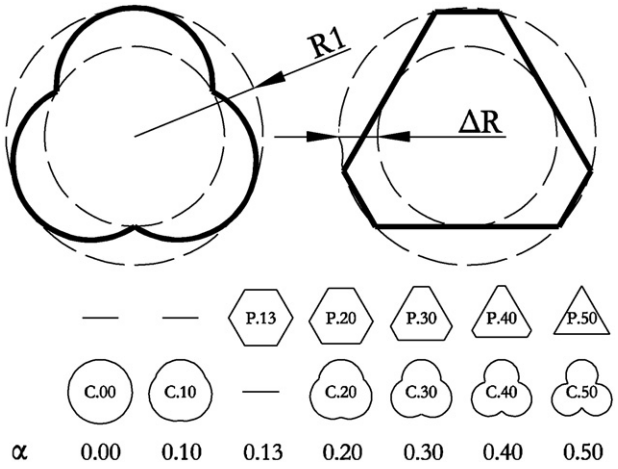

Fig. 1. Particle shape definition: $\alpha = \frac{\Delta R}{R_1}$ and examples of clump and polygon particle shapes used.

contact force f_n is related to the normal interpenetration (or overlap) h of the contact

$$f_n = k_n \cdot h \quad , \tag{1}$$

as f_n vanishes if contact disappears, i.e. $h = 0$. The tangential component f_t of the contact force is proportional to the tangential elastic relative displacement, according to a stiffness coefficient k_t. The Coulomb condition $|f_t| \leq \mu\, f_n$ requires an incremental evaluation of f_t in every time step, which leads to some amount of slip each time one of the equalities $f_t = \pm \mu f_n$ is imposed (μ corresponds to the contact friction coefficient). A normal viscous component as opposed to the relative normal motion of any pair of grains in contact is also added to the elastic force f_n. Such a term is often introduced to facilitate the mechanical equilibrium approach [14]. In case of frictional assemblies under quasi-static loading, the influence of this viscous force (which is proportional to the normal relative velocity, using a damping coefficient g_n) is not significant [15] (elastic energy is mainly dissipated by Coulomb friction). Finally, the motion of grains is calculated by solving Newton's equations using either a leap-frog (in PFC^{2D}) or third-order predictor–corrector discretisation scheme [16] (in the in-house software). This constitutes the only known difference between the two codes.

The principles of disc contact detection are well known [13,17], and contact detection for clumps was solved in the same way: contact occurs at a point, the normal force value f_n is calculated with Eq. (1) and its direction connects the centers of discs in contact, Fig. 2(a). Contact detection and contact force calculations between polygons do not use classical methods based on the area overlap between polygons [18–21]. The *shadow overlap* technique proposed by J.J. Moreau [22], which was originally applied within the *Contact Dynamic* approach [23] for convex polygonal particles, was used. In our study this technique was adapted to the MD approach. Three types of geometrical contact can exist between polygons: Corner-to-Corner, Corner-to-Edge (*CE*) and Edge-to-Edge (*EE*). Corner-to-Corner contacts are geometrically (or mathematically) realistic but never occur in our simulations because of the numerical rounding errors. When dealing with (*EE*) contact, contact detection involves two contact points and their associated overlaps h, Fig. 2(b). This is the main difference compared to the classical method (area overlap

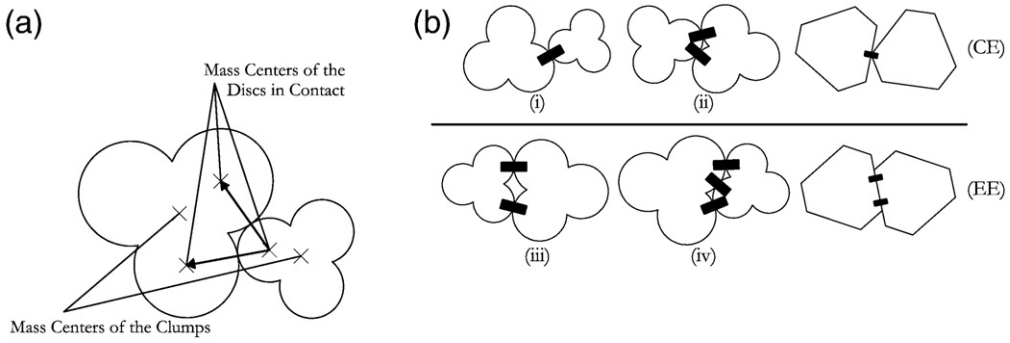

Fig. 2. Contacts between the particles; contact definition and classification. (a) Definition of a contact between clumps. Normal contact vector connects the centers of the discs in contact. (b) Various types of possible contacts between clumps. Analogy between clump and polygon contacts: corner-to-edge (CE) and edge-to-edge (EE) groups. Note that for a contact between two polygon edges two contact points are considered while only one if there is a contact between a corner and an edge.

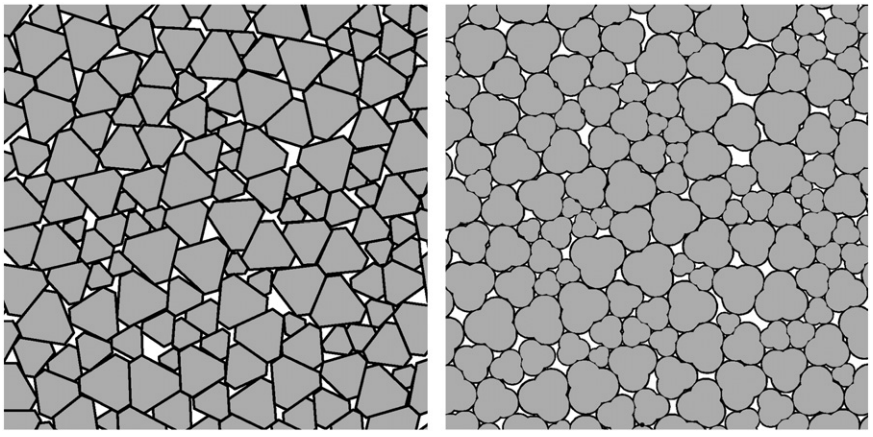

Fig. 3. Fragments of two confined dense samples with $\alpha = 0.3$. Sample $P_D.30$ on the left and $C_D.30$ on the right.

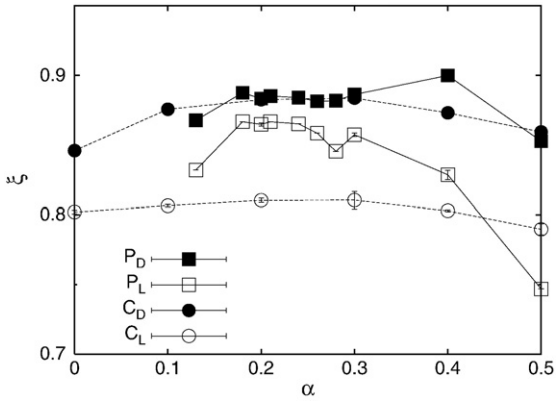

Fig. 4. Solid fraction ξ of the samples under isotropic loading versus α. Error bars correspond to standard deviation calculated using of four samples. The round and square symbols represent samples made of clumps and polygons, respectively. The black and white symbols represent dense and loose samples, respectively. This convention will be maintained hereafter.

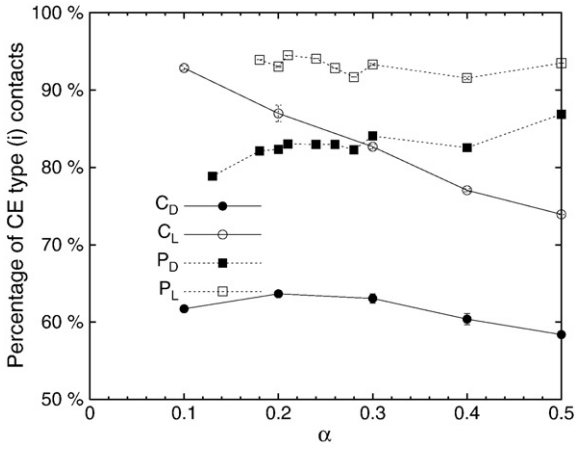

Fig. 5. Corner-to-edge contacts ((CE) see Fig. 2(b)) percentage in the isotropic state, ε_i. Comparison between clumps and polygons.

calculations) where only one contact is considered between the edges.

Finally, we may be interested in the main contact law parameters: the normal and tangential stiffness, k_n and k_t, and the friction coefficient μ. Assuming that samples would first be loaded with a 2D isotropic stress $\sigma_0 = 10$ kN/m, the normal stiffness of contact k_n was calculated according to the dimensionless 2D *stiffness parameter* $\kappa = k_n/\sigma_0$ [15,24–26]. κ expresses the mean level of contact deformation, $1/\kappa = h/\langle 2R\rangle$, where $\langle R\rangle$ is the mean particle radius. In our simulations, κ was arbitrarily set to 1000. As a comparison, a sample made of glass beams under isotropic loading of 100 kPa reaches $\kappa = 3000$. The tangential stiffness k_t can be expressed as a fraction of the normal stiffness, $\tilde{k} = k_t / k_n, \tilde{k} > 0$. $\tilde{k} > 1$ may exhibit specific behaviour where *Poisson coefficient* of grain assemblies become negative [27–30]. Running several numerical simulations with various $\tilde{k}$, $0 < \tilde{k} \leq 1$, [25] have shown that if $0.5 \leq \tilde{k} \leq 1$, the macroscopic behaviour remains similar. Thus we arbitrarily set $\tilde{k}$ to 1.

4. Sample preparation — isotropic compression

Granular samples of 5000 grains are prepared in three steps: preparations start with a random spatial distribution of particle position inside a square made of four rigid walls. Secondly, the particles expand slowly until $\sigma_0 = 0.5$ kN/m is reached. Finally, samples are isotropically loaded by wall displacement up to $\sigma_0 = 10$ kN/m. To obtain samples with different solid fractions, we may use various values of the intergranular friction coefficient μ during the preparation [31]. When μ is set to zero, samples isotropically loaded up to $\sigma_0 = 10$ kN/m are dense and the Solid fraction is *maximal*. When a strictly positive value of μ is used instead, samples become looser and Solid fraction decreases. In our study dense samples were prepared with $\mu = 0$ and the loose ones with μ equal 0.5. 16 different samples (4 dense, 4 loose made of clumps and 4 dense, 4 loose made of polygons) for each α value were prepared.[1] Dense samples will be written as C_D or P_D respectively for Clumps and Polygons. Loose samples will be denoted as C_L or P_L . A subscript can be added. It then corresponds to the decimal part of the shape number α. As an example, fragments of two dense samples with $\alpha = 0.30$, $C_D.30$ and $P_D.30$, are displayed in Fig. 3.

For both clumps and polygons, contact between particles can occur at more than one contact point. There are four contact possibilities for clumps: single contact Fig. 2(b)(i) double contact involving three discs Fig. 2(b)(ii), double contact involving four discs Fig. 2(b)(iii) and triple contact Fig. 2(b) (iv). By analogy with polygon contacts (Edge-to-Edge or Corner-to-Edge, Fig. 2(b)), all these contacts between clumps can be merged into two groups, (*CE*) and (*EE*). In the (*CE*) group, grains involved in a single contact (i) may rotate without sliding. Double contact (ii) allows rotation with sliding and eventually friction. Rotation and sliding of polygons meeting at a single contact point are not correlated. Group (*EE*) contacts block the rotation of the grains. In the case of rotation of grains, contacts of this type would be lost. Therefore, the shape of the grains can be regarded as macro roughness.

For samples subjected to isotropic loading, we focus on two internal parameters that mainly determine the mechanical behaviour: the Solid fraction ξ and the coordination number z^*. Fig. 4 shows the evolution of ξ with α for dense and for loose samples. For C_D samples, ξ evolution is bell-shaped and maximum Solid fraction is reached for $0.2 \leq \alpha \leq 0.3$. Similar observations were made by [9,10]. This also seems to be the case for C_L samples although the amplitude of the bell-shaped curve appears to be lower. The geometrical origin of these results deals with the grain shape (concavity and grains envelope) and imbrication and the interlocking between grains, but appears to be complex to establish. While we might think that when two grains are in contact with a single point of contact (contact (*CE*)-*type* (*i*), Fig. 2(b)), this would tend to increase the local porosity and thus reduce the overall Solid fraction; this does not seem to be the case:

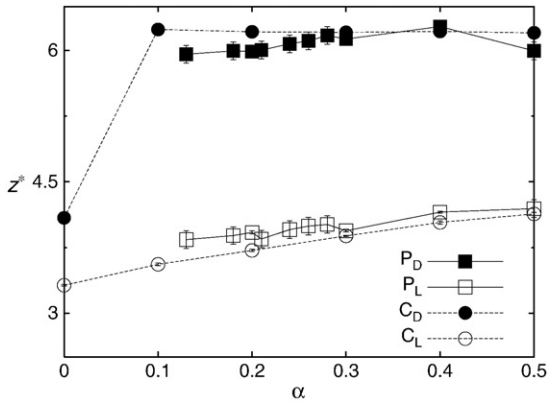

Fig. 6. Coordination number z^* values vs. α under isotropic loading. The round and square symbols represent samples made of clumps and polygons, respectively. The black and white symbols represent dense and loose samples, respectively.

[1] All the analyses presented in this article were carried out on mean results calculated over 4 samples of each density and each α. Associated Standard Deviations will always be given, even if they are too small to be significant.

Fig. 5 shows clearly that for C_D samples, the proportion of contact (*CE*)-*type* (*i*) is at its maximum for $0.2 \leq \alpha \leq 0.3$ in the case of dense samples and decreases linearly with α in the case of C_L samples. This completely goes against the ξ trend, even if it is clearly established that when ξ is high (C_D samples), the proportion of (*CE*)-*type* (*i*) contacts is lower than in the case where the Solid fraction is low (C_L samples).

For samples made of polygons, the dependence of ξ on α is not clear either. For P_D samples, ξ is almost constant for $0.2 \leq \alpha \leq 0.3$. If we exclude the P_D.40 sample, which behaves in a peculiar way, we can notice that for samples made of grains with regular shapes, corresponding to $\alpha = 0.13$ and $\alpha = 0.5$, the Solid fraction ξ is smaller than for samples made of grains which have shape irregularities ($0.13 < \alpha < 0.5$). The relationship between ξ and the percentage of (*CE*)-*type* (*i*) contact is again impossible to establish. Furthermore, it is worth observing that when $0.2 \leq \alpha \leq 0.3$, C_D and P_D samples show very similar Solid fraction. Here, grain envelope seem to be a cleverer interpretation of α parameter than grain imbrication, which is only relevant for clumps. Finally, we should note that the angle of friction used during the preparation does not seem to have a major influence on the Solid fraction of samples made of polygons when $0.2 < \alpha < 0.3$.

For samples subjected to isotropic loading, we studied the *coordination number* z^* corresponding to the mean number of contacts per grain. Here only grains that have two or more compression forces, and therefore take part in the load transfer, were considered. For samples made of frictionless perfectly rigid discs, $z^* = 4$ [32]. Because κ is not infinite in our study, in the samples made of frictionless circular particles (C_D.00), $z^* = 4.093 \pm 0.005$ is greater but still very close to the reference value. z^* is evaluated for clumps and polygons and both dense and loose samples. The dependence of z^* according to α is shown in Fig. 6. For C_L samples, z^* increases linearly with α, like P_L samples, but for C_L , it can be directly correlated to the percentage of (*CE*)-*type* (*i*) contacts which decrease with α, and then increase z^*. For dense samples, the percentage of (*CE*)-*type* (*i*) contacts did not vary too much. z^* is constant for C_D and P_D samples.

5. Macromechanical response of granular assembly loaded in vertical compression test

The samples were tested in a 2D strain controlled vertical compression test, also called *biaxial test*. Vertical stress σ_1 was applied by increasing the compressive vertical strain ε_1 while lateral σ_3 remained constant. The loading velocities were chosen according to the dimensionless *inertial number* $I = \dot{\varepsilon}_1 \sqrt{\frac{\langle m \rangle}{\sigma_3}}$ [26] where $\dot{\varepsilon}_1$ denotes the strain rate and $\langle m \rangle$ the typical mass of a grain. It describes the level of dynamic effects in the sample. For quasi-static evolutions, the value of I should be low. I value was set to $5 \cdot 10^{-5}$ for clumps and for polygons samples, regardless of the code used. During the vertical compression in both dense and loose samples, the same value of contact friction coefficient $\mu = 0.5$ was used. The mechanical responses of the samples are plotted on η vs. ε_1 charts and shown in Fig. 7. $\eta = t/s$, $t = (\sigma_1 - \sigma_3)/2$ is half of the deviator stress and $s = (\sigma_1 + \sigma_3)/2$ is the mean stress. Extracted from $\eta - \varepsilon_1$ curves shown in Fig. 7, friction angles at the peak ϕ_p and at the threshold ϕ_t are given Fig. 8(a). Average dilatancy angles extracted from Fig. 9 are presented in Fig. 8(b).

For dense samples made of clumps, C_D , we can observe in Fig. 7(a) that the macroscopic shear resistance increases with α. Although

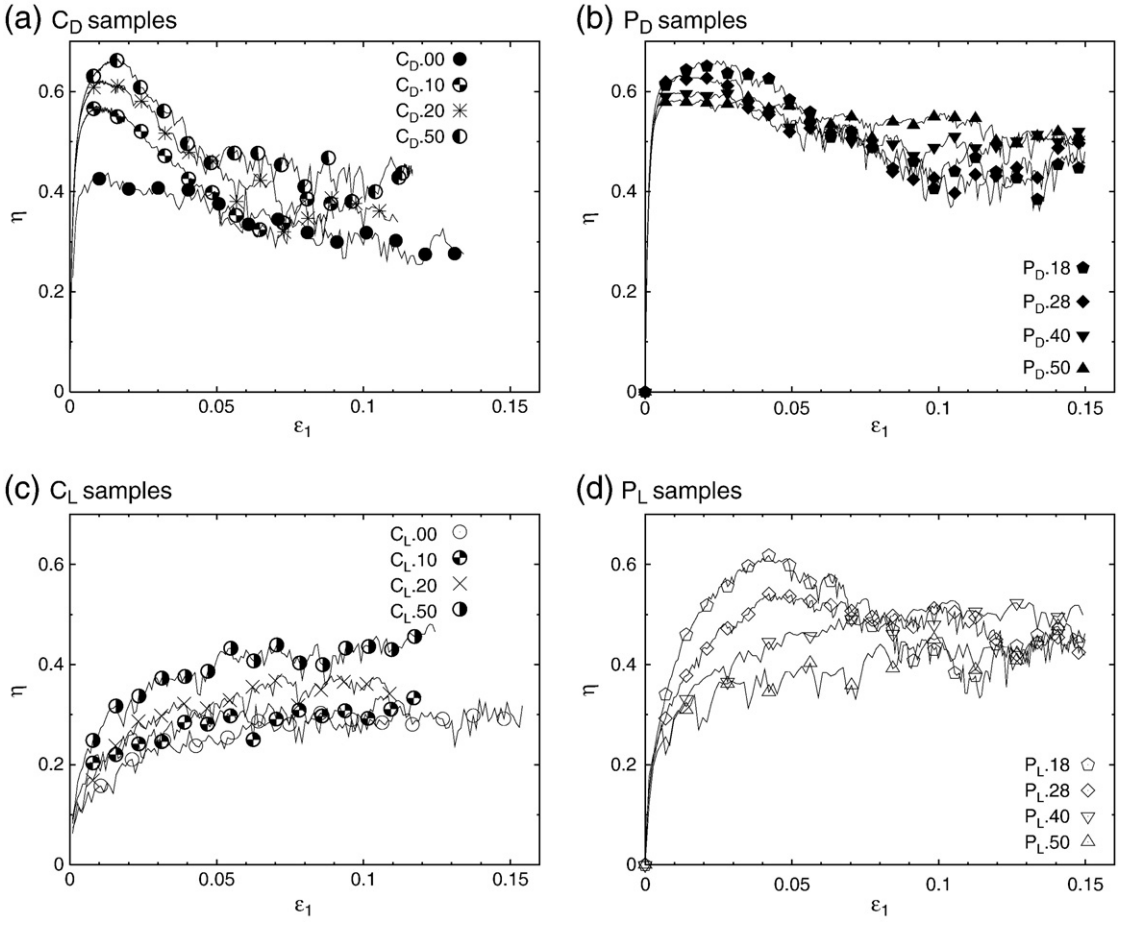

Fig. 7. Macroscopic $\eta - \varepsilon_1$ curves for some of the samples.

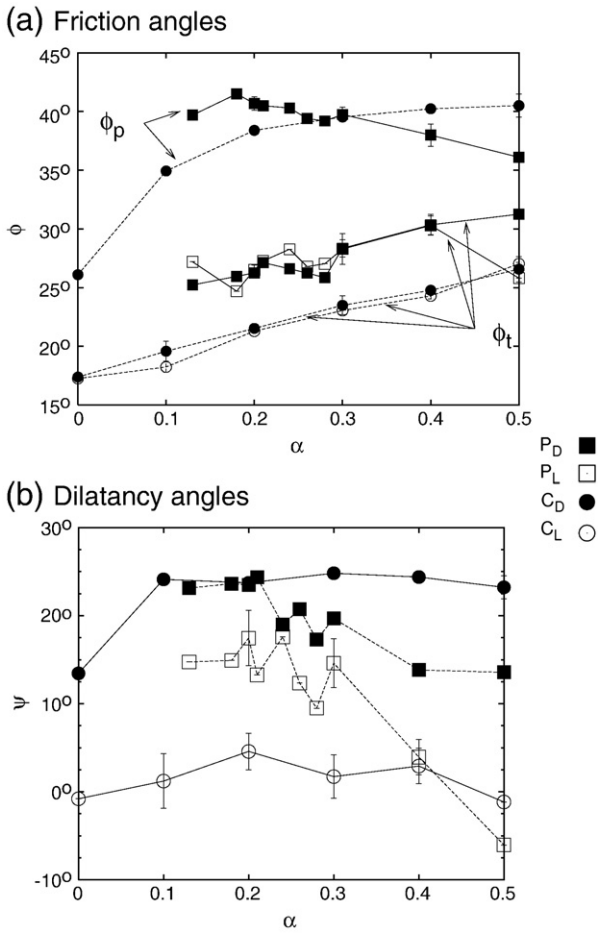

Fig. 8. (a) Friction angles vs. α for clumps and polygons samples. The two upper curves correspond to friction angles at the peak ϕ_p of dense samples. The four other curves show friction angles at the threshold ϕ_t, either for dense or loose samples. (b) Dilatancy angles for all the samples; Values of the angles for dense samples were calculated at the peak, between [1.5–2.5%] ε_1; For loose ones, the range was [6–7%] ε_1.

C_D.10 implies grains with a small α, the mechanical response of the sample exhibits remarkable increase of the maximum deviator in comparison to disc samples C_D.00 where rotations of particles are not potentially disturbed by the grain shape. For C_L samples, there is no peak value of the friction angle, $\phi_p = \phi_t$, Fig. 7(c). Thus, for all clump samples, both peak ϕ_p and threshold ϕ_t friction angle values increase along with α. ϕ_t increases proportionally with α while the increase of ϕ_p is nonlinear and seems to be asymptotic for $\alpha \geq 0.4$.

For P_D samples, ϕ_p values slightly decrease linearly along α, while ϕ_t values increases, Fig. 8(a).

For P_L samples, we can notice in Fig. 7(d) that the macroscopic curves show typical behaviour similar to that of loose samples when $\alpha < 0.3$ and a typical behaviour characteristic of dense samples for $\alpha > 0.3$. This kind of behaviour deals with the values of the initial Solid fraction of the samples shown in Fig. 4 where we can observe that ξ values for P_D and P_L samples are very close when $\alpha \leq 0.3$. If we focus only on ϕ_t for P_L samples, we can observe (Fig. 8(a)) an increase of the friction angle with α, except for samples made of triangles, $\alpha = 0.5$, which always behave in a specific way.[2] In conclusion, it can be noted that adding some shape irregularity by increasing α always leads to an increase of the macroscopic angle of friction in the critical state. This is the case for clumps and polygons with a constant microscopic friction angle μ.

[2] Note that triangle is the only shape with 3 edges.

This influence of grain geometry is in line with a previous study by Salot et al. [7]. Lastly, as we can see in Fig. 7, α does not explicitly influence Young's modulus. E is linked to the rigidity matrix and therefore to z^* [33], which is constant for dense samples (Fig. 6).

Similarly, particle concavity does not particularly influence the average dilatancy angle ψ values $\left(\sin\psi = \frac{d\varepsilon_1 + d\varepsilon_3}{d\varepsilon_1 - d\varepsilon_3}\right)$ of dense and loose clump samples (Fig. 8(b)). On the other hand, ψ is lower for polygons with higher values of α (closer to triangular shape) than for those more similar to hexagons.

In Fig. 9, volumetric changes in some samples are illustrated. For both dense clump and polygon samples, Fig. 9(a) and (b), the volume[3] increases mainly during vertical compression, after a small contraction due to the stiffness of the contacts [15]. The volumetric increase for C_D samples is quite similar from one α to another (Fig. 9(a)). On the other hand, α clearly influences the volumetric change of P_D samples but this influence seems erratic. Nevertheless, P_D samples show greater total dilatancy than C_D samples. C_L samples (Fig. 9(c)) behave like loose sands and contract all throughout the compression test. It is more complex for P_L samples (Fig. 9(d)) for which the setting-up process remains problematic for some values of α.

6. Micromechanical analysis

From the macroscopic results exposed in the previous section, two main observations can be established: for dense samples made of clumps, the evolution of the angle of friction at the stress peak ϕ_p varies significantly with α. The geometrical imbrication between grains in contact, which depend on α, may be one of the micromechanical origins of these results. Secondly, for all samples, dense or loose, made of clumps or polygons, it was established that the angle of friction ϕ_t at the end of biaxial tests increases with α and is independent of the initial state. This result is a proof of the role of the grain envelope in the mechanical behaviour rather than some inter-granular imbrication considerations. In this section we will try to gather evidence for these proposals.

6.1. Contact proportion evolution for dense samples made of clumps

Single contacts are mainly involved in all the grains samples tested, Fig. 5 ((*CE*) contacts for polygons or (*CE*)-*type* (*i*) contacts for clumps — Fig. 2(b)). During loading, it can be noted that the percentage of single contacts increases. Because dense samples were prepared with no friction, Solid fraction of each assemblies of grains subjected to isotropic loading is constant and always maximal. As a consequence, even if samples can exhibit slight contractancy (related to dimensionless contact stiffness κ, [34]), the total number of contacts in each sample during a vertical compression systematically decreases. Therefore, in order to compare different contact type proportions in different phases of the test, we suggest balancing the decrease in the total number of contacts using the coefficient $\omega^* = N^*_{\varepsilon_b}/N^*_{\varepsilon_a}$. $N^*_{\varepsilon_a}$ and $N^*_{\varepsilon_b}$ represent the total number of neighbouring contacts[4] at the given vertical strains ε_1 (ε_a or ε_b) in the samples. Here, we suggest focusing on the evolution of two new contact groups for clumps:

- (*SC*) single contact between grains, known as *simple* contact,
- (*CC*) multiple contacts between grains, hereafter called *complex* contacts.

These two new groups can be examined in Fig. 10.

We observed the evolution of clump contact numbers of each group between two successive stages by normalising this evolution

[3] For convenience we resort to the vocabulary pertaining to 3D triaxial tests.

[4] When two grains are in contact via 1, 2 or 3 contact points, only one contact is counted.

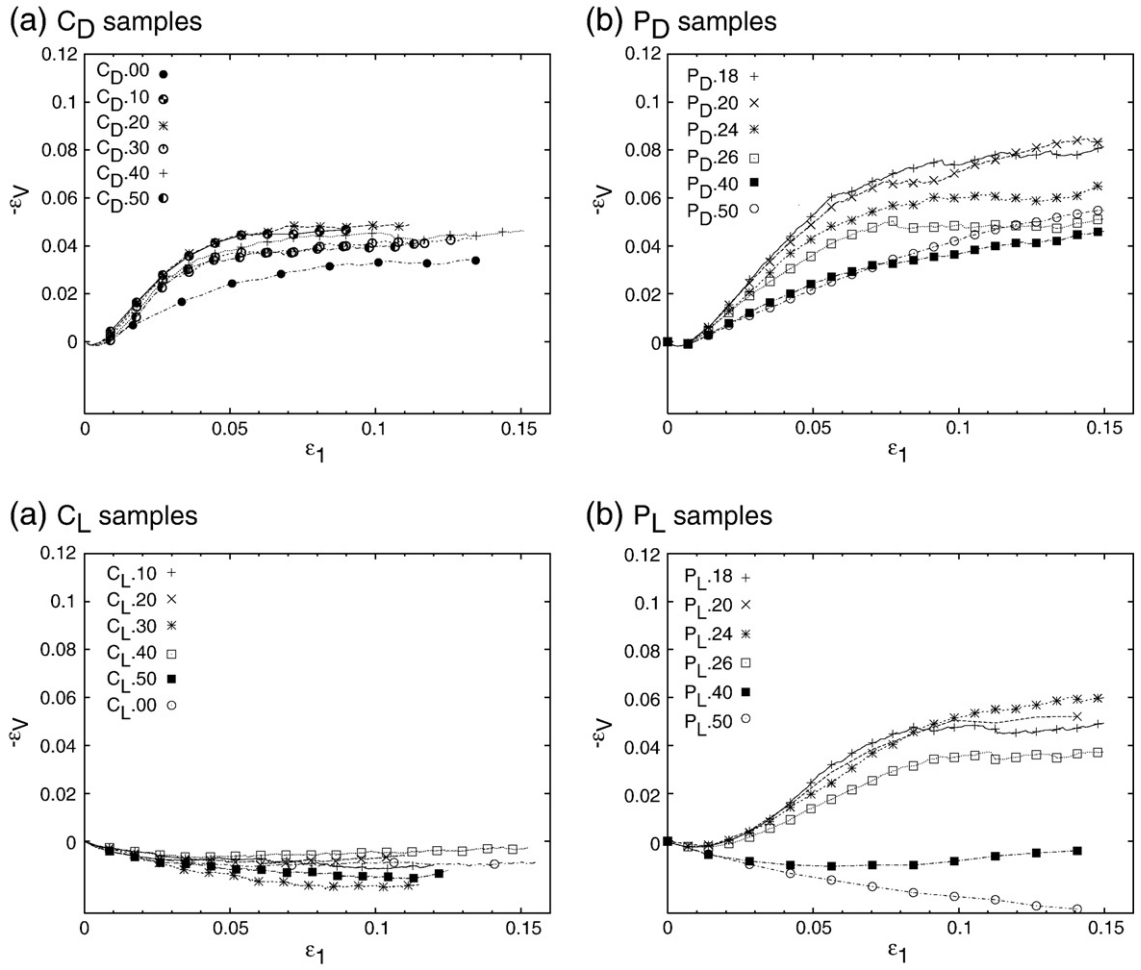

Fig. 9. Volumetric changes (computed in 2D corresponding to the area) during vertical compression for loose and dense samples made of clumps and of polygons. Positive $-\varepsilon_v$ implies an increase of the sample volume.

with ω^*. We thus defined a new variable $\lambda = \omega^* \cdot N_{\varepsilon_a}/N_{\varepsilon_b}$, where N_{ε_a} and N_{ε_b} denote the number of (*SC*) or (*CC*) on two different levels ε_a and ε_b of the vertical strain ε_1. In Fig. 11(a), λ evolution is calculated between $\varepsilon_a = \varepsilon_i$ (isotropic state) and $\varepsilon_b = \varepsilon_p$ (maximum stress deviator). We can observe that for $\alpha = 0.10$, λ is smaller than 1 for (*CC*) and greater than 1 for (*SC*). This can be regarded as a transformation of (*CC*) into (*SC*) between these two stages. If all the complex contacts transformed into simple, graphic points were at an equal distance from 1, $1-\lambda_{(CC)} = \lambda_{(SC)} - 1$. If $1-\lambda_{(CC)} > \lambda_{(SC)} - 1$, it means that some complex contacts transform into simple contacts but some of them also disappear.

When α goes to 0.5, these transformations are still active but with less intensity. Geometrical imbrications between clumps increase with α and are "more difficult to lose" during the biaxial tests. It is also interesting to observe that λ seems to reach a threshold when $\alpha \geq 0.4$, Fig. 11(a). This last observation can be correlated to the evolution of ϕ_p, which also reaches a threshold for the same value of α, Fig. 8(a).

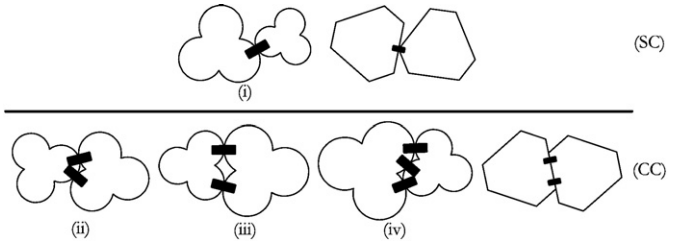

Fig. 10. Contact types for clumps and polygons: simple contacts (SC) and complex contacts (CC).

Focusing on λ between the peak and the critical state, $\varepsilon_a = \varepsilon_p$ and $\varepsilon_b = \varepsilon_c$, Fig. 11(b), we can observe that the increase of simple contacts is small for every α ($\lambda_{(SC)} - 1 \leq 0.1$) and complex contacts are mainly lost $1-\lambda_{(CC)} > 0.1$, especially when α is small. The greater α is, the smaller the proportion of complex contacts lost (grain imbrications are destroyed less). This may be a clue that ϕ_t of clumps increases with α, as seen in Fig. 8(a). Nevertheless, some new investigations on the evolution of contact orientations are proposed in the next section.

6.2. Evolution of contact fabric for C_D samples

Contact direction and its evolution during the vertical compression tests are often analysed [35]. Focusing on the first part of the mechanical behaviour, from the isotropic state to the stress peak for example, it is well known that in dense samples, contacts are mainly lost in the extension direction and gained in the direction of compression, [36]. In Fig. 12(a) to (d), for two values of α, we present statistical analysis of the evolution of contact direction by the evaluation of $\mathcal{P}(\theta) = N_{\varepsilon_b}(\theta) / N_{\varepsilon_a}(\theta)$, where ε_a and ε_b correspond to two successive vertical strains levels and where $N_{\varepsilon_x}(\theta)$ is the number of contacts in the direction θ. $\mathcal{P}(\theta) = 1$ expresses that the number of contacts in the direction θ remains constant between the two configurations studied. If $\mathcal{P}(\theta) = <1$, contacts are lost and if $\mathcal{P}(\theta) > 1$,

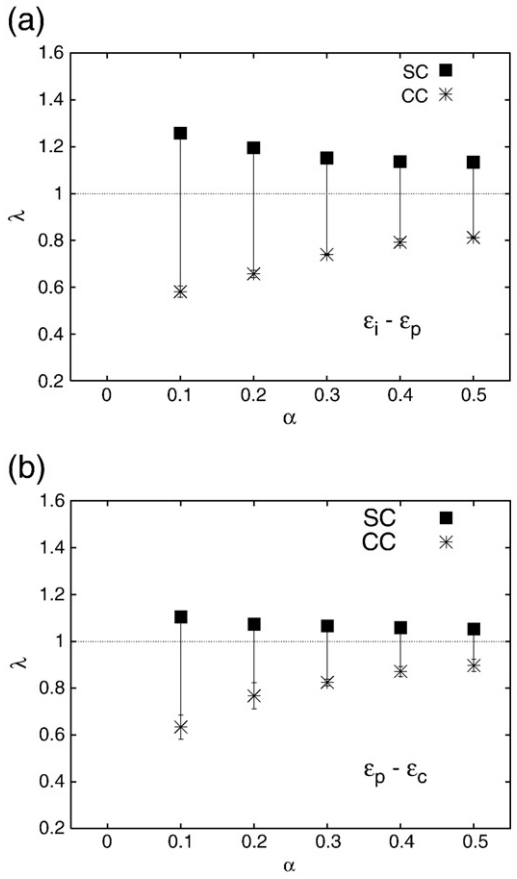

Fig. 11. Transformation of complex clump contacts into simple contacts, quantified by λ and evaluated between the ε_i and ε_p for figure (a), and between ε_p and ε_c for figure (b).

contacts are gained in the direction θ. Integrated over θ, $\langle\mathcal{P}\rangle$ is a global evaluation of the proportion of gained or lost contacts.

We focus on the evolution of contact anisotropy between the isotropic state and the peak, Fig. 12(a) for $\alpha=0.2$ and Fig. 12(c) for $\alpha=0.5$, we can observe that there is no contact gain in any direction: in the compression direction, the number of contacts remains constant $\mathcal{P}(\theta)\simeq 1$ and the number of contacts decreases in the extension direction $\mathcal{P}(\theta)<1$. The mean value of $\mathcal{P}$ over θ is smaller than 1 for both α discussed here and also for the other α studied. During the vertical compression of C_D , sample contacts are mainly lost. Finally, we noticed that the greater α is, the smaller the amount of contacts lost in the extension direction. By analysing the contacts change in direction between the peak and the critical state, ε_p to ε_c, Fig. 12(b) and (d), opposite tendencies emerge: contacts are mainly lost in the compression direction and gained in the extension direction, with a less intensive effect for $\alpha=0.5$, Fig. 12(d). At this stage of analysis, we are not yet able to distinguish the nature of the contacts involved in these observations. An analysis of clustered contacts, as outlined below, is thus necessary.

We now suggest the same contact direction analysis but for (*SC*) and (*CC*) groups (simple and complex contacts). Statistical analysis of the evolution of contact orientation from the isotropic state ε_i to the peak ε_p for (*SC*) and (*CC*) groups is shown in Figs. 12(e) to (h). On one hand, Fig. 12(e) and (f) show that in the compression direction (*SC*) contacts are gained ($\alpha=0.2$) or are kept ($\alpha=0.5$). (*SC*) contacts are mainly lost in the extension direction, with a more pronounced amplitude when α is small. On the other hand, we can observe that (*CC*), Figs. 12(g) and (h), are lost in every direction with some variations depending on θ. Nevertheless, complex contacts are more persistent when α is greater ($\langle\mathcal{P}\rangle$. is greater for $\alpha=0.5$ because of grain imbrications).

The statistical analysis of the evolution of contact direction between the peak ε_p and the critical state ε_c shown in the Figs. 12(i) to (l) confirms the tendency shown in Figs. 12(b) and (d): simple and complex contacts are lost in the compression direction. For (*SC*) with $\alpha=0.2$, $\langle\mathcal{P}\rangle=1$, Fig. 12(i): although the number of (*SC*) decreases in the compression direction and increases in the extension direction, the number of simple contacts remains constant during the mechanical test from the peak to the critical state. When $\alpha=0.5$, the number of simple contacts decreases $\langle\mathcal{P}\rangle=0.9$, especially in the compression direction. Complex contacts are the ones that are lost the most ($\langle\mathcal{P}\rangle$ is always lower than 1, regardless of the value of α). Nevertheless, it is desirable to make a distinction based on α: the amount of (*CC*) lost is smaller for $\alpha=0.5$ ($\langle\mathcal{P}\rangle=0.8$, Fig. 12(k)) than for $\alpha=0.2$ ($\langle\mathcal{P}\rangle=0.7$, Fig. 12(l)). The proportion of (*CC*) lost in the compression direction is bigger for $\alpha=0.2$, like if vertical contact chains were more unstable or less persistent when α tends to 0.

Further studies, taking into account the intensity of contact forces and their propensity to be stronger in the case of complex contacts [37] would provide more certainty about possible links between the observations made above and improvement of the mechanical property ϕ_t measured at ε_c, Fig. 8(a).

6.3. Evolution of comparative contact proportions in compression tests for clumps and polygons

Focusing on the critical phase only, contact observations are now based on the division into two contacts groups corner-to-edge (*CE*) and edge-to-edge (*EE*) (Fig. 2(b)). The evolution of (*CE*) contacts according to α is shown in Fig. 13. (*EE*) contacts can be easily deduced by subtracting (*CE*) contacts percentage from 100%. On one hand, the percentage of (*CE*) contacts does not depend on the initial Solid fraction of the sample; dense and loose samples exhibit a similar trend. On the other hand, (*CE*) contact percentages for C_D and C_L samples decrease linearly with α. A different tendency is observed for P_D and P_L samples where the contact percentage remains more or less the same except for $\alpha=0.5$. We can even observe that when $\alpha=0.5$, (*CE*) contacts and (*EE*) contact percentages are close: for this special value of α, clump and polygon envelopes converge.

6.4. Influence of shape on local strain analysis

We focused on the strain localisation in the samples in order to study the macroscopic rupture and its origin. Two approaches were used: *local strain maps* and *shear localisation indicator* S_2 [38]. By comparing particle kinematics in the isotropic state $\varepsilon_1=\varepsilon_i=0$ and in the deformed stage ε_1, we calculated local strains using Delaunay triangulation as in [36] (Delaunay triangle corners correspond to the mass centers of particles). Using the second strain invariant, $I_{\varepsilon_d}=\varepsilon_I-\varepsilon_{II}$, where ε_I and ε_{II} are respectively the major and the minor principal strains, we illustrate the shear localisation in Fig. 14. We should notice that such shear localisation patterns, also called shear bands, are often observed on granular materials confined by more or less rigid boundaries, or even numerical or experimental considerations [36,39–41]. Even if the number of shear bands depends on the macroscopic strain levels applied to samples, different patterns (multiple shear zones) seem to exist when periodic boundary conditions are used [42].

The shear localisation indicator S_2 is defined as

$$S_2 = \frac{1}{N_t}\frac{\left(\sum_{i=1}^{N_t} I_{\varepsilon_d}\right)^2}{\sum_{i=1}^{N_t} I_{\varepsilon_d}^2} \quad , \tag{2}$$

where I_{ε_d} is the second invariant of the strain tensor and N_t is the total number of Delaunay triangles. In a sense, value of S_2 can be regarded as a percentage of a distorted sample area.

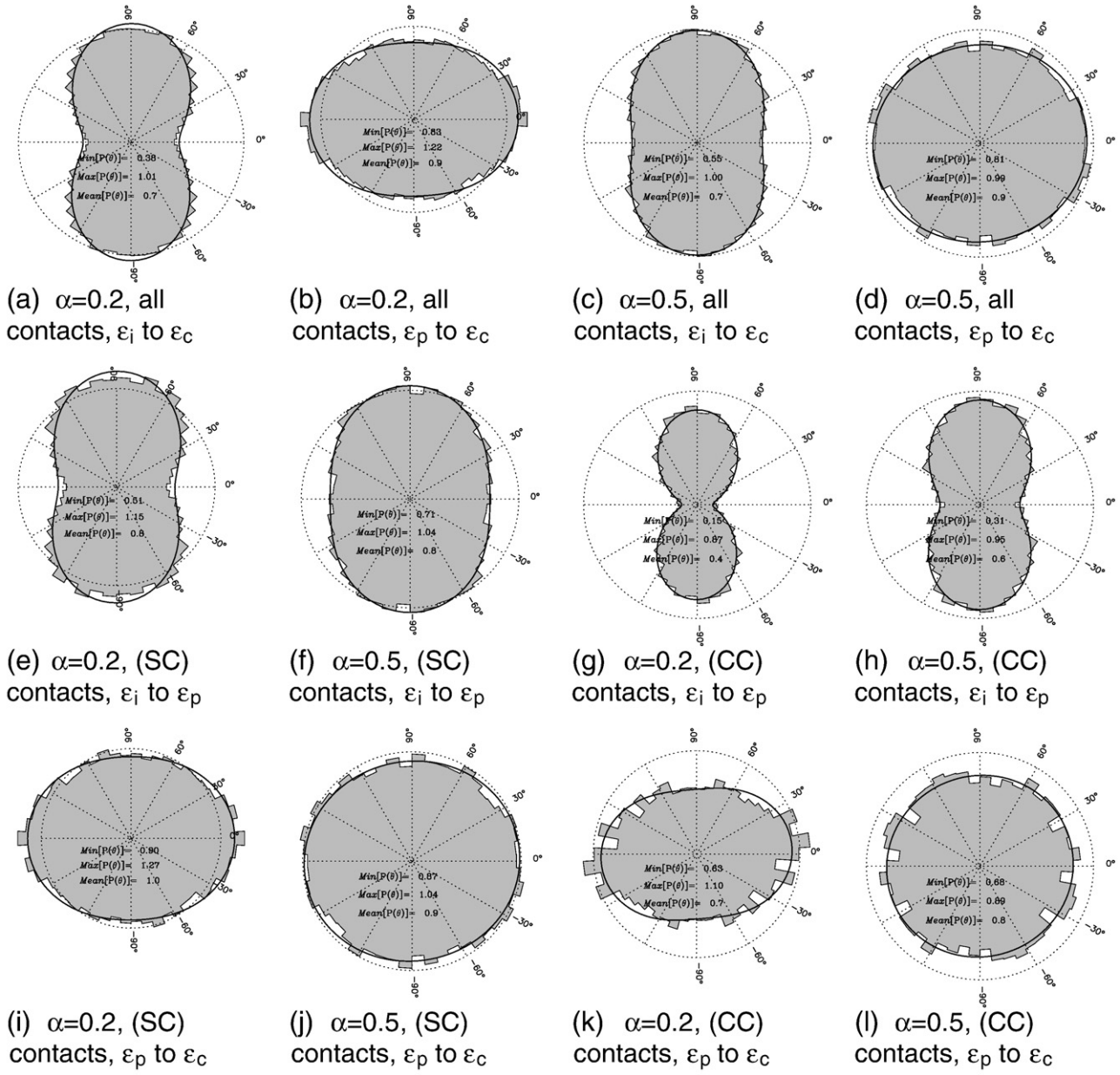

Fig. 12. C_D samples. Histogram analysis of the evolution of contact directions for all the contacts (panels (a) to (d)) or for (*SC*) and (*CC*) (panels (e) to (l)). Histograms calculated over 25 classes of 7.2° each, between two successive strains levels: ε_i to ε_p for the panels (e) to (h) and ε_p to ε_c for the figures (i) to (l). When all the contacts are taken into account (panels (a) to (d)), the statistics are calculated over approximately 40,000 contacts for the isotropic state, 30,000 contacts at the peak and 29,000 at the critical state. The circle radius drawn in dashed line is 1.

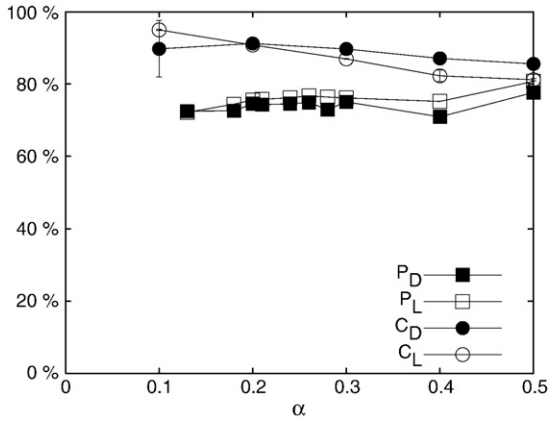

Fig. 13. Corner-to-edge contacts ((*CE*) see Fig. 2(b)) percentage at critical state, ε_c. Comparison between clumps and polygons.

Fig. 15 gives the evolution of S_2 according to ε_1 for several dense and loose samples made of clumps and polygons. Regardless of the sample studied, the sheared area always reaches a maximum which is at least greater than 50%. From evolution of S_2, we may encounter two types of behaviour: samples for which S_2 reaches a maximum and then decreases and stabilises, and a second type where S_2 increases asymptotically towards a maximum.

We have observed that when S_2 reaches a maximum and later decreases to reach a threshold value, it always corresponds to samples which were identified as dense samples because $\phi_p > \phi_t$ (for example C_D.50 , P_D.24 , P_L.28 samples of the Fig. 14). On the contrary, when $\phi_p \sim \phi_t$, samples can be classified as loose samples. In this case, S_2 continuously increases from $\varepsilon_1 = 0$ to 10% to eventually reach a threshold close to $S_2 \simeq 60\%$.

In the case of dense samples, the asymptotic value of S_2 is interesting because it clearly shows higher values for P_D samples than for C_D samples. Coupling this quantitative result with the qualitative

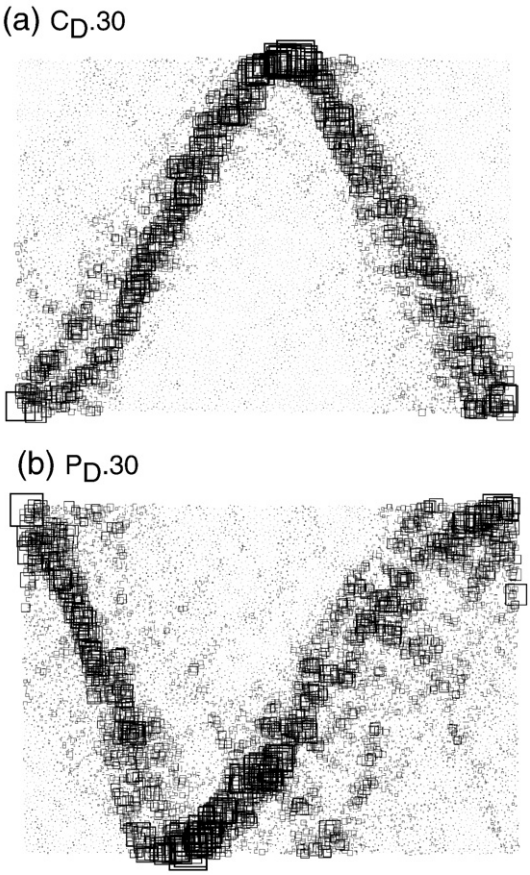

Fig. 14. Shear maps on dense samples made of grains with $\alpha = 0.3$ calculated from the isotropic state to $\varepsilon_1 = 13.5\%$. Black square symbols are proportional to the amplitude of the second invariant of the strains I_{ε_d}.

observation of shear maps like in the Fig. 14, it is obvious that localised zones in P_D samples are wider than in C_D samples. This result is consistent with the overall dilatancy of samples: P_D samples globally expand more than C_D ones. For loose samples, the sheared area always corresponds to approximately 60% of the samples, regardless of the grain shape.

7. Conclusions and discussion

The aim of this article was to present some new investigations on the mechanical influences of particle shape in granular assemblies in the framework of numerical simulations performed with Discrete Element Method. First, a grain geometry parameter α was defined by the CEGEO research team. For particles called clumps, made of 3 overlapping discs, α is a measure of the grain concavity. 6-edged convex polygonal grains were also ruled by α. The overall envelope depending on α for each type of particles used in the studied granular model was the common feature. Our numerical simulations were performed with the Discrete Element Method adapted to each grain shape. For particles made of discs (clumps), the commercial code PFC^{2D} by ITASCA was used. For polygonal particles, we developed our own computer code which implements special contact detection between objects in the framework of Molecular Dynamic approach. In this article, we highlighted that changing the grain geometry, influences granular assembly mechanical behaviour under the classical vertical compression test in 2D. More complex grain shapes allow higher levels of internal friction angle and large volumetric strains to be reached compared to simple discs. Some clear differences in the behaviour of polygon (convex) and clump (non-convex) assemblies were shown. We should also note that the particle shapes chosen also demonstrate similarities, caused by the global envelope, that justify the comparison. The generation and compaction of granular assemblies were presented. By using two extreme values of the inter-granular friction angle μ, dense and loose samples were prepared, both for samples made of clumps and polygons.

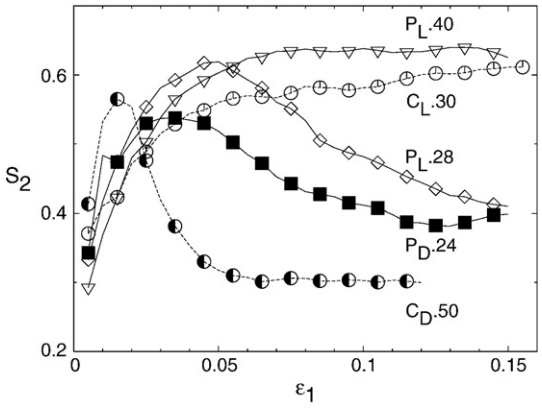

Fig. 15. Shear indicator evolution during a vertical compression.

Firstly, by focusing on the macroscopic mechanical behaviour of our granular model we show that loose samples composed of polygons with low values of α present behaviour typical to moderately dense granular samples. For these granular materials, the initial contracting stage was not only due to contact stiffness, but was also influenced by large inter-granular reorganisation. Apart from this, loose and dense samples of all shapes behaved as expected (loose samples only show contracting behaviour while dense ones mostly exhibit major dilatancy), showing similar behaviour when discussing friction residual angles ϕ_t or contact percentages. All samples show higher values of internal friction angles ϕ_p and ϕ_t than samples made of only circular grains where each particle is a disc. The correlations between shape parameter α and friction angles are different for clumps and polygons. On one hand, for dense clump samples ϕ_p increases with α and seems to reach an asymptotic value $\phi_p = 40^\circ$. On the other hand, ϕ_p linearly decreases when α shifts from 0.13 to 0.5. In this case, the particular case of the triangular shape ($\alpha = 0.5$) is also discussed briefly. The overall dilatancy of clump samples is greater than that of disc assemblies, but spectacularly smaller than dilatancy of polygons.

Secondly, on the granular scale, we suggested correlating macroscopic observations by means of contact evolution analysis, which led us to introduce several groups of contacts between particles. Thus, we observed that multiple contacts between clumps transform into simple contacts and that this process depends on the size of concavities, i.e. α. We tend to associate this with an increase of shear resistance in the case of dense granular samples made of clumps. However, for a better understanding of the role of α in the magnitude of contact forces and their influence on the macroscopic repercussions, complementary studies need to be carried out.

Focusing on granular assembly failure, we studied the localisation of shear bands and tried to characterise it by a scalar. It was observed that reflecting shear bands were thinner in dense samples made of clumps than in those made of polygons, regardless of the α type, thus highlighting the evident effects of the geometrical imbrications of clumps. Polygon samples gradually create wide shear bands, while for samples made of clumps, the appearance of shear bands are more immediate.

Although the meaning and implications of the parameters α have been presented in this article, it needs to be clarified further. Nevertheless, from the comparisons between polygons and clumps, two trends seem to emerge: for very dense samples made of clumps, a large α naturally implies imbrications between particles. α is thus a

measure of clump concavity. With the simulations exposed in this article, we can deduce that the larger the concavities are, the higher the angle of friction at the peak ϕ_p is.

For the samples made of polygons, this does not apply. Indeed, there are no imbrications between the grains and α is thus a measure of grain sphericity. We have shown that in dense samples made of polygons, the percentage of a single contact in the isotropic state increases with α. In corollary, we can observe that the angles of friction peak decrease slightly with α.

For loose samples P_L or C_L, or for P_D and C_D samples close to the critical state, ϕ_t is the parameter which characterises the failure. We have shown that for large strains, contacts between grains are mostly single. Therefore, clump imbrications are less involved in the evolution of ϕ_t. Furthermore, ϕ_t, which increases linearly with α, increases with the same rate regardless of the grain shape. α should thus be only regarded as a parameter of spherical grains.

Acknowledgments

This study was carried out as part of a CEGEO research project (http://www.granuloscience.com/CEGEO/). The authors would like to express special thanks to F. Radjai, C. Nouguier for fruitful discussions and to F. Nicot for his very useful suggestions. The authors are indebted to J.J. Moreau for his guidance on algorithm for contact detection between polygon objects.

References

[1] J. Lanier, M. Jean, Experiments and numerical simulations with 2D-disks assembly, Powder technology (special issue on Numerical simulations of discrete particle systems) 109 (2000) 206–221.
[2] C. Thornton, J. Lanier, Uniaxial compression of granular media: numerical simulations and physical experiment, in: R.P. Behringer, J. Jenkins (Eds.), Powders and Grains 97, Balkema, Rotterdam, 1997, pp. 223–226.
[3] M. Oda, K. Iwashita (Eds.), Mechanics of Granular Materials, An Introduction, A.A. Balkema, ISBN: 90-5410-461-9, 1999.
[4] K. Iwashita, M. Oda, Rotational resistance at contacts in the simulation of shear band development by DEM, ASCE Journal of Engineering Mechanics 124 (1998) 285–292.
[5] A. Tordesillas, D.C. Stuart, Incorporating rolling resistance and contact anisotropy in micromechanical models of granular media, Powder Technology 124 (2002) 106–111.
[6] F. Gilabert, J.-N. Roux, A. Castellanos, Computer simulation of model cohesive powders: influence of assembling procedure and contact laws on low consolidation states, Physical Review E (Statistical, Nonlinear, and Soft Matter Physics) 75 (2007) 011303.
[7] C. Salot, P. Gotteland, P. Villard, Influence of relative density on granular materials behavior: DEM simulations of triaxial tests, Granular Matter 11 (4) (2009) 221–236.
[8] E. Azema, F. Radjai, R. Peyroux, G. Saussine, Force transmission in a packing of pentagonal particles, Physical Review E (Statistical, Nonlinear, and Soft Matter Physics) 76 (1) (2007) 011301.
[9] B. Saint-Cyr, C. Voivret, D.J.-Y., F. Radjai, P. Sornay, Effect of shape nonconvexity on the shear strength of granular media, in: Powders and grains 2009, AIP Conference Proceedings, Materials Physics & Applications, vol. 1145, Golden, CO USA, 2009, pp. 389–392.
[10] K. Szarf, G. Combe, P. Villard, Influence of the grains shape on the mechanical behavior of granular materials, in: Powders and grains 2009, AIP Conference Proceedings, Materials Physics & Applications, vol. 1145, Golden, CO USA, 2009, pp. 357–360.
[11] D. Rapaport, The Art of Molecular Dynamics Simulation, Cambridge University Press0-521-82568-7, 1995.
[12] Itasca Consulting Group Inc., PFC^{2D}, Particle Flow Code in Two Dimensions-User's Guide, Itasca Consulting Group Inc., 1999.
[13] P.A. Cundall, O.D.L. Strack, A discrete numerical model for granular assemblies, Géotechnique 29 (1) (1979) 47–65.
[14] A. Atman, P. Claudin, G. Combe, Departure from elasticity in granular layers: investigation of a crossover overload force, Computer physics communications 180 (4) (2009) 612–615.
[15] J.-N. Roux, G. Combe, On the meaning and microscopic origins of "quasistatic deformation" of granular materials, Proceedings of the EM03 ASCE conference, CD-ROM published by ASCE, Seattle, 2003.
[16] M. Allen, D. Tildesley, Computer simulation of liquids, Oxford Science Publications, 1994.
[17] S. Luding, Stress distribution in static two-dimensional granular model media in the absence of friction, Physical Review E (Statistical, Nonlinear, and Soft Matter Physics) 55 (4) (1997) 4720–4729.
[18] M. Hopkins, On the ridging of intact lead ice, Journal of Geophysical Research 99 (C8) (1994) 16,351-16,360.
[19] H.-G. Matuttis, Simulation of the pressure distribution under a two-dimensional heap of polygonal particles, Granular matter 1 (2) (1998) 83–91.
[20] F. Alonso-Marroquin, S. Luding, H.J. Herrmann, I. Vardoulakis, The role of the anisotropy in the elastoplastic response of a polygonal packing, Physical Review E (Statistical, Nonlinear, and Soft Matter Physics) 71 (2005) 051304.
[21] F. Alonso-Marroquin, H.J. Herrmann, Calculation of the incremental stress-strain relation of a polygonal packing, Physical Review E (Statistical, Nonlinear, and Soft Matter Physics) 66 (2) (2002) 021301, doi:10.1103/PhysRevE.66.021301 http://dx.doi.org/10.1103/PhysRevE.66.021301.
[22] J. Moreau, Private communication (2006).
[23] G. Saussine, C. Cholet, P.-E. Gautier, F. Dubois, C. Bohatier, J. Moreau, Modelling ballast behaviour under dynamic loading. Part 1: A 2D polygonal discrete element method approach, Computer Methods in Applied Mechanics and Engineering 195 (2006) 2841–2859.
[24] G. Combe, J.-N. Roux, Discrete numerical simulation, quasitatic deformation and the origins of strain in granular materials, in: H. DiBenedetto, T. Doanh, H. Geoffroy, C. Sauzeat (Eds.), 3rd International Symposium on Deformation Characteristics of Geomaterials, Lyon, France, 2003, pp. 1071–1078.
[25] G. Combe, http://pastel.paristech.org/00000051/Origines microscopiques du comportement quasi-statique des matériaux granulaires, Ph.D. thesis, École Nationale des Ponts et Chaussées, Champs-sur-Marne, France (2001). URL http://pastel.paristech.org/00000051/.
[26] J.-N. Roux, F. Chevoir, Discrete numerical simulation and the mechanical behavior of granular materials, Bulletin des Laboratoires des Ponts et Chaussées 254 (2005) 109–138.
[27] B. Emeriault, B. Cambou, A. Mahboudi, Homogenization for granular materials: non reversible behaviour, Mechanics of cohesive-frictional materials 1 (1996) 199–218.
[28] B. Cambou, P. Dubujet, F. Emeriault, F. Sidoroff, Homogenization for granular materials, European J. of Mechanics A/Solids 14 (1995) 255–276.
[29] J. Bathurst, L. Rothenburg, Micromechanical aspects of isotropic granular assemblies with linear contact interactions, Journal of Applied Mechanics 55 (1988) 17–23.
[30] J. Bathurst, L. Rothenburg, Note on a random isotropic granular material with negative poisson's ratio, International Journal Engineering Science 26 (1988) 373–383.
[31] B. Chareyre, P. Villard, Dynamic spar elements and DEM in two dimensions for the modeling of soil-inclusion problems, Journal of Engineering Mechanics 131 (2005) 689–698.
[32] I. Agnolin, J.-N. Roux, Internal states of model isotropic granular packings. I. Assembling process, geometry, and contact networks, Physical Review E (Statistical, Nonlinear, and Soft Matter Physics) 76 (6) (2007) 061302.
[33] I. Agnolin, J.-N. Roux, Internal states of model isotropic granular packings. III. Elastic properties, Physical Review E: Statistical, Nonlinear, and Soft Matter Physics 76 (6) (2007) 061304.
[34] J.-N. Roux, G. Combe, Quasistatic rheology and the origins of strain, Comptes Rendus de l'Académie des Sciences, Série IV - Physics-Astrophysics (Comptes Rendus Physique) 3 (2) (2002) 131–140.
[35] R. Behringer, J. Jenkins (Eds.), Powders and Grains 97 — International Conference on Powders & Grains — (3rd — 1997 — Durham, N.C., USA), A.A. Balkema, Rotterdam, 1997.
[36] F. Calvetti, G. Combe, J. Lanier, Experimental micromechanical analysis of a 2D granular material: relation between structure evolution and loading path, Mechanics of Cohesive-frictional materials 2 (1997) 121–163.
[37] E. Azéma, F. Radjaï, R. Peyroux, Force transmission in a packing of pentagonal particles, Physical Review Letter 76 (2007) 011301.
[38] A. Sornette, P. Davy, D. Sornette, Fault growth in brittle–ductile experiments and the mechanics of continental collisions, Journal of geophysical research 98 (1993) 12111–12140.
[39] J. Lanier, Étude expérimentale des lois de comportements en grandes déformations à l'aide d'une presse réellement tridimensionnelle, Cahier du groupe français de Rhéologie 4 (1976) 53–57.
[40] J. Lanier, M. Jean, Experiments and numerical simulations with 2D-disks assembly, Power Technology 109 (2000) 206–221.
[41] J. Desrues, G. Viggiani, Strain localization in sand: an overview of the experimental results obtained in Grenoble using stereophotogrammetry, International Journal for Numerical and Analytical Methods in Geomechanics 28 (2004) 279–321.
[42] M. Kuhn, K. Bagi, Specimen size effect in discrete element simulations of granular assemblies, Journal of Engineering Mechanics 135 (2009) 485–492.